



UNIVERSITEIT•STELLENBOSCH•UNIVERSITY  
jou kennisvenoot • your knowledge partner

*Comparison of PM vernier and conventional synchronous 15 kW wind generators  
(repository copy)*

---

**Article:**

Tlali, P.M., Wang, R-J., Gerber, S., (2018) Comparison of PM vernier and conventional synchronous 15 kW wind generators, *XXIII International Conference on Electrical Machines*, (ICEM), pp. 2065--2071, 3-6 September 2018, Alexandroupoli, Greece

<http://dx.doi.org/10.1109/ICELMACH.2018.8506882>

---

**Reuse**

Unless indicated otherwise, full text items are protected by copyright with all rights reserved. Archived content may only be used for academic research.

# Comparison of PM Vernier and Conventional Synchronous 15 kW Wind Generators

P. M. Tlali, R.-J. Wang and S. Gerber

**Abstract**—This paper presents the 2D finite element analysis (FEA) based design optimization of a surface-mounted permanent magnet vernier machine (PMVM), and its comparison against the permanent magnet synchronous machine (PMSM) in a 15 kW wind generator application. The PMVM's operating principle is briefly discussed, and attention is given to the selection of the number of stator slots, armature poles and rotor poles in order to achieve low active mass and good torque quality. The designed PMVM is also compared to a benchmark PMSM in terms of, amongst others, torque per mass, torque density, torque quality and power factor, by utilizing 2D FEA. It is concluded that the PMVM can be a competitive alternative to the PMSM in this application.

**Index Terms**—Design optimization, finite element analysis, flux modulation, magnetic gearing effect, permanent magnet, vernier machines

## I. INTRODUCTION

WITH the steady growth of the global demand for wind energy, the size and output capacity of wind turbines have also been increasing over years [1]. This requires larger generators that can handle high torques and convert most of the power captured by the turbine blades. A key challenge is that both the volumetric size and total mass of the generator have maximum limits imposed by, among other factors, the material cost and the tower's maximum weight support and vibrational handling capability. Thus, mechanically geared medium/high speed generator systems are still popular options although they are prone to reliability issues. However, for applications with serviceability issues (e.g. offshore wind farms), directly driven generators (DDGs) remain a favored option despite their known heavy weights and large sizes in comparison to the geared systems. For power electronic converter (PEC) interfaced grid connection, PM synchronous machines (PMSM) are arguably the most promising type of DDGs because of their better efficiency and relatively good torque density [2], [3].

In the past decade, the permanent magnet vernier machine (PMVM) has emerged as an attractive alternative to either DDGs or geared generator systems. By virtue of the magnetic gearing principle inherent in them, PMVMs render superior

torque density than PMSM while they also have similar structural simplicity [4], [5]. There has been some comparative studies previously made between these two machine types [6]–[8]. Most of these studies followed a traditional method of comparison whereby the output power or torque density is optimized within a fixed machine volume.

The aim of this paper is to design and compare a PMVM with an existing PMSM machine. To facilitate this, the principles of the PMVM are briefly reviewed in section II, and the candidate PMVM types described in section III. Then an FEA design optimization is done on several pole/slot combinations as presented by section IV. The primary objective of the optimization was to minimize the electromagnetic active mass, while the other performance parameters such as torque and power factor are also taken into consideration. Consequently, one best pole/slot combination is chosen to be further analyzed in section V, with the same rated output conditions as the benchmark PMSM. Based on the 2D FEA, the performance results of these two machines are then compared to give an indication into the prospects of the PMVM becoming a substitute of the PMSM in direct drive applications.

## II. OPERATING PRINCIPLES OF PMVMs

The operational principle of the PMVM is mainly based on the *magnetic gearing effect*. As in magnetic gears, the high-speed PM poles are magnetically coupled to the low-speed PM poles through modulation by the ferromagnetic pole-pieces. In PMVMs, the high speed field harmonics are produced by the armature currents, while the low-speed poles are created by the rotor PMs. To enable the magnetic gearing effect, the number of ferromagnetic pole pieces ( $N_s$ ), armature magnetic pole-pairs ( $p_s$ ) and rotor PM pole-pairs ( $p_r$ ) must satisfy the following relationship [4], [9]:

$$N_s = p_r \pm p_s \quad (1)$$

By assuming that the iron relative permeability is infinite, and that the PMs are uniformly magnetized in the radial direction, the open-circuit air-gap flux density distribution along the angular periphery of the rotor ( $\theta$ ) can then be described as [4], [9], [10]:

$$B_{PM}(\theta, t) = F_{PM}(\theta, t) \times \Lambda(\theta) \quad (2) \\ \cong [F_{PM1} \cos \{p_r(\theta - \omega_r t)\}] \times [\Lambda_0 - \Lambda_1 \cos(N_s \theta)]$$

where  $F_{PM}$  and  $\Lambda$  are the PMs magneto-motive force (MMF) distribution and the air-gap permeance function, respectively. For analysis purposes, the effects of high order harmonics

---

This work was supported in part by ABB Corporate Research, Sweden and the Stellenbosch University in South Africa.

P. M. Tlali, R.-J. Wang and S. Gerber are with the Department of Electrical and Electronic Engineering, Stellenbosch University, Stellenbosch 7600, South Africa (e-mail: 15894215@sun.ac.za; rwang@sun.ac.za; sgerber@sun.ac.za)

may be ignored. It suffices to approximate  $B_{PM}$  with just the average and the fundamental harmonic components of both the  $F_{PM}$  and  $\Lambda$ , which then gives the expression below:

$$B_{PM}(\theta, t) \cong B_{PM0} \cos \{p_r(\theta - \omega_r t)\} - \frac{B_{PM1}}{2} \left\{ \begin{aligned} &\cos \{(N_s - p_r)\theta - p_r \omega_r t\} \\ &+ \cos \{(N_s + p_r)\theta - p_r \omega_r t\} \end{aligned} \right\} \quad (3)$$

where  $B_{PM0} = F_{PM1} \Lambda_0$   $B_{PM1} = F_{PM1} \Lambda_1$

On examining (3) in conjunction with (1), it can be seen that the resultant air-gap flux density distribution has three major components, being the term that has equal harmonic order and rotates synchronously with the PM rotor and the two other terms produced by the modulation effect of the ferromagnetic pole-pieces. It is important to realize that one of these modulated terms bears similar spacial period to the fundamental component of armature coil current MMF. Thus, the engagement of these two field harmonic components results in steady torque transmission between the rotor and stator, even-though they have different number of pole-pairs.

Integrating (3) relative to the angular distance of the armature coil would give the per phase open-circuit flux linkage. Consequently, the change of flux-linkage with respect to time results into the induced electro-motive force (EMF).

$$E_{ph(rms)} = K_{w1} N_{ph} D_g l_{stk} \omega_r \left[ B_{PM0} + \frac{p_r}{p_s} \frac{B_{PM1}}{2} \right] \quad (4)$$

with  $\frac{d}{dt} \theta_r = \omega_r$

where  $D_g$ ,  $l_{stk}$  and  $K_{w1}$  are the air-gap diameter, machine stack length and the fundamental winding factor, respectively. The presence of two voltage components is now evident in the developed voltage expression. The first term is equivalent to the component found in classical synchronous machines, while the second term is due to the vernier effect. With the pole-pairs' and ferromagnetic pole-pieces' numbers chosen according to (1), the two EMF components add up together contributing to larger voltage production [4]. With the induced voltage and per phase current ( $I_{ph}$ ) known, the air-gap torque for a three-phase PMVM is then formulated as shown by (5). It can be clearly seen from (5) that a PM rotor to stator magnetic pole-ratio ( $p_r/p_s$ ) also appears to proportionately increase the torque:

$$T_q = K_{w1} N_{ph} I_{ph} D_g l_{stk} \left[ B_{PM0} + \frac{p_r}{p_s} \frac{B_{PM1}}{2} \right] \quad (5)$$

### III. CONSIDERED PMVM CONFIGURATIONS

PMVMs can be realized into various configurations characterized by different performance merits. The current study focused on the three common single-stator single-rotor PMVMs shown in Fig. 1. Furthermore, the choice of number of stator slots and rotor pole-pairs is very important as this determines the machine speed gear ratio ( $G_r$ ) and operating frequency for a given input speed. Generally, the suitable  $G_r$  can be chosen on the basis of the intended/required speed and/or torque conversion factor, while also taking

into consideration the predicted torque quality of each pole-slot combination. As a preliminary design exercise to find a suitable pole-ratio to work with, a survey was taken whereby a series of 3 kW PMVMs with various pole/slot combinations and pole-ratios were optimized under the same design constraints. Again, in order to select the best PMVM configuration, the optimization was done for three different PMVM types, namely:

- PMVM (conventional overlap-winding) (Fig. 1a)
- Split-tooth PMVM (tooth concentrated winding) (Fig. 1b)
- Separate modulator PMVM (tooth concentrated winding) (Fig. 1c)

All the investigated pole/slot combinations are provided in Tables I and II for overlap-winding and tooth concentrated machines, respectively. Considered machine designs were selected to have gearing ratios ( $G_r$ ) spanning from 5 up to 20 increasing in steps of 3, and the number of stator pole-pairs are 1, 2 and 3.

It should also be realized that while the number of stator slots or teeth ( $Q$ ) is the same as the number of modulating pieces ( $N_s$ ) in conventional overlap-winding PMVMs, this is a different case in the other PMVM types. In tooth concentrated-winding machines, the number of modulator pieces is chosen with regard to (1), as it is the case with the number of stator teeth in overlap-winding machine. The designer further has to separately choose the number of stator slots, which in combination with the stator pole-pairs, will have the best possible winding factor, as outlined in other studies for this winding type [11], [12]. In addition, the number of stator slots must be a factor of the modulator pole-pieces in tooth-split PMVMs. However, this restriction can be automatically removed by adopting the separate modulator tooth concentrated winding PMVM structure, since the modulator and stator are two separate components.

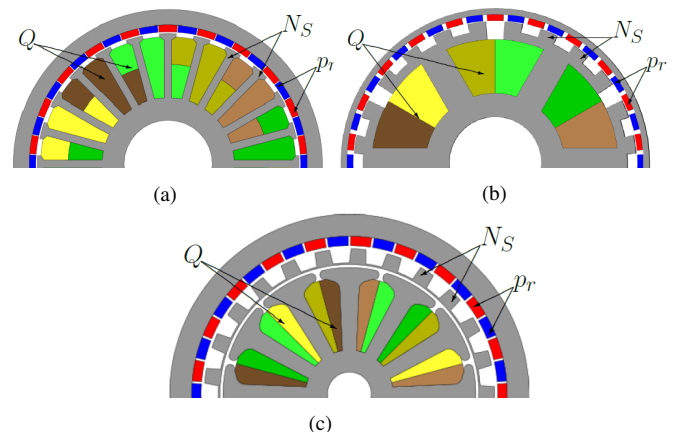


Fig. 1. Considered PMVM types: (a) Conventional overlap-winding PMVM (b) Tooth concentrated, split tooth PMVM (c) Tooth concentrated, separate modulator PMVM.

TABLE I  
INVESTIGATED POLE-SLOT COMBINATIONS FOR OVERLAP-WINDING PMVMS.

$p_s$	Pole-ratio = 5			Pole-ratio = 8			Pole-ratio = 11			Pole-ratio = 14			Pole-ratio = 17			Pole-ratio = 20		
	Q	$p_r$	q	Q	$p_r$	q	Q	$p_r$	q	Q	$p_r$	q	Q	$p_r$	q	Q	$p_r$	q
1	6	5	1.0	9	8	1.5	12	11	2.0	15	14	2.5	18	17	3.0	21	20	3.5
2	12	10	1.0	18	16	1.5	24	22	2.0	30	28	2.5	36	34	3.0	42	40	3.5
3	18	15	1.0	27	24	1.5	36	33	2.0	45	42	2.5	54	51	3.0	63	60	3.5

TABLE II  
INVESTIGATED POLE-SLOT COMBINATIONS FOR TOOTH CONCENTRATED-WINDING PMVMS.

$p_s$	Pole-ratio = 5				Pole-ratio = 8				Pole-ratio = 11				Pole-ratio = 14				Pole-ratio = 17				Pole-ratio = 20			
	Q	$N_s$	$p_r$	q	Q	$N_s$	$p_r$	q	Q	$N_s$	$p_r$	q	Q	$N_s$	$p_r$	q	Q	$N_s$	$p_r$	q	Q	$N_s$	$p_r$	q
1	3	6	5	0.5	3	9	8	0.5	6	12	11	1.0	3	15	14	0.5	9	18	17	1.5	3	21	20	0.5
2	6	12	10	0.5	9	18	16	0.75	12	24	22	1.0	15	30	28	1.25	6	36	34	0.5	21	42	40	1.75
3	9	18	15	0.5	9	27	24	0.5	18	36	33	1.0	9	45	42	0.5	27	54	51	1.5	9	63	60	0.5

#### IV. DESIGN OPTIMIZATION

The objective of the overall optimization process was to minimize the machines' total active mass for a fixed output power for different pole-slot combinations. All the machines must have an output power of 3 kW with at least 90% efficiency at the rated speed of 150 rpm. The modified method of feasible directions (MMFD) algorithm in VisualDOC optimization suite from VR&D Inc. [13] was employed for the optimization. VisualDOC is coupled with an in-house FEM program through the external scripts files. The optimization process was performed with a 2D FE static analysis of the machine with a current angle of 90 degrees. The constrained optimization problem was formulated as follows:

$$\begin{aligned} \text{Minimize: } & F(\mathbf{X}) = M_{\text{Total}} \\ \text{Subject to: } & \eta \geq 90\% \quad \text{and} \quad J \leq 4 \text{ A/mm}^2 \end{aligned}$$

where  $\mathbf{X}$  represents the vector of geometric variables in Fig. 2 with angle ratios defined in (6).

$$\begin{aligned} \theta_{pm\_p} &= \frac{\pi}{p_r}; & \theta_{sp} &= \frac{2\pi}{Q} \\ \sigma_{pm} &= \frac{\theta_{pm\_s}}{\theta_{pm\_p}}; & \sigma_s &= \frac{\theta_s}{\theta_{sp}}; & \sigma_{so} &= \frac{\theta_{so}}{\theta_s} \end{aligned} \quad (6)$$

During the optimization process, core-losses, end-winding length, end-winding's inductance and resistances were calculated using analytical equations so that their effect can be included in the performance evaluation deduced from 2D

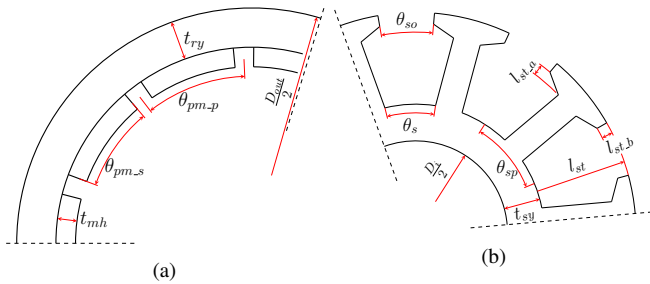


Fig. 2. Machine geometric optimization variables: (a) Rotor (b) Stator.

FEA static solutions. Thus, both the efficiency and power factor calculations have included the effect of end-windings. In addition, the grade and material type for PMs, iron, and windings are kept the same across all the candidate machines. The main parameters that define the objective search space for each considered machine are provided in Table III below. A stator slot fill factor of 0.45 was assumed.

##### A. Electromagnetic Active Mass

The total active masses as a function of the gear ratios for the three PMVM configurations are quantitatively compared in Fig. 3. It can be observed that as the gear ratio increases, the total active mass initially decreases before this downward trend ceases at certain gear ratio, after which the mass stays constant or even increase again. The reason for this, is that the higher gear ratio means large number of rotor pole-pairs, which encourages excess PM leakage flux and consequently the poor performance. In addition, higher gear ratio also implicates high operational frequency for the same input speed, which results in increased core losses. Since the minimum efficiency requirement has to be fulfilled in the optimization, a design with high core loss would respond by increasing the rotor and stator yokes to reduce flux density magnitudes in the affected regions, leading to heavier designs.

Another noticeable trend is that combinations with  $p_s = 1$  generally lead to the heaviest designs due to their thick stator and rotor yokes. For overlap-winding machines with stator magnetic pole-pairs equal to 2 and 3, the mass begins to be constant at  $G_r$  of 11 and upwards, whereas it slowly increases for tooth concentrated machines. It can also be noted that the results in Fig. 3 partly differ to the analytical equations based predictions which neglects the effect of component partial saturation and flux leakage.

TABLE III  
MAIN SPECIFICATIONS FOR THE OPTIMIZED MACHINES.

Parameter	Value
Output power (kW)	3
Air-gap length (mm)	0.8
Slot-fill factor	0.45
Operating speed (rpm)	150
Aspect ratio ( $\frac{L}{D}$ )	0.05 - 0.7

L = active stack length, D = outer diameter.

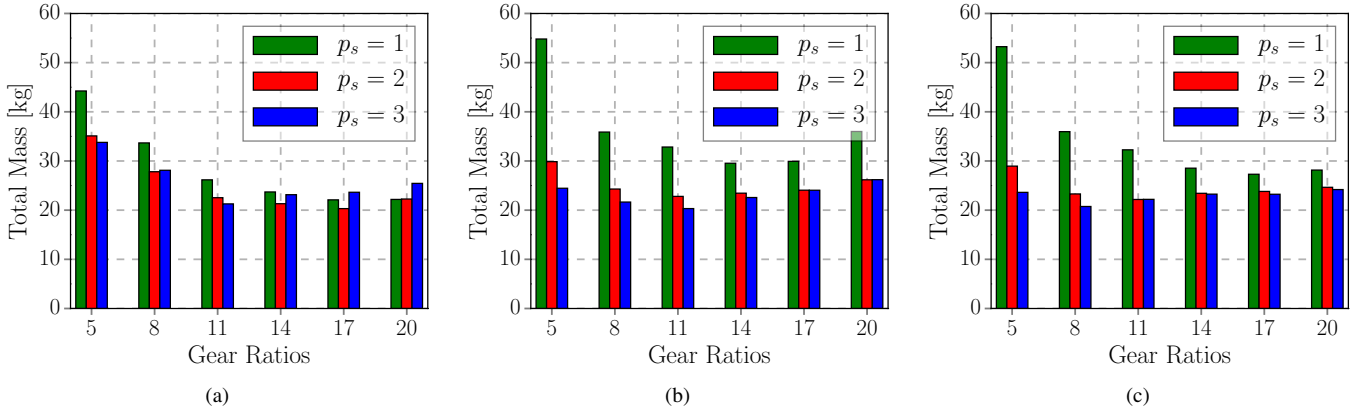


Fig. 3. Total active mass vs Gear ratio.: (a) Conventional overlap-winding PMVM (b) Tooth concentrated, split tooth PMVM (c) Tooth concentrated, separate modulator PMVM.

### B. Power Factor

When considering the power factor, Fig. 4 shows that it doesn't necessarily follow a uniform trend against the rising gear ratio, although on average, most machines on the high end have lower power factor than those on the lower side of the  $G_r$  scale. This phenomenon can be better explained by the simplified power factor expression (7), whereby the pole-ratio appears on the denominator of the equation [14]. Consequently, it can be realized that the power factor has an indirect inverse proportionality to the gear ratio.

$$X_{sg} = \omega_r p_r L_{gs} = \omega_r \frac{p_r}{p_s} \frac{m}{2} \frac{\pi \mu_o N_{ph}^2 l_{stk} D_g}{4 p_s g} K_{w1} \quad (7)$$

$$P_f = \frac{1}{\sqrt{1 + \left( \frac{X_{sg} I_{ph}}{E_{ph}} \right)^2}}$$

where  $P_f$ ,  $L_{gs}$  and  $X_{sg}$  are the power factor, synchronous inductance and reactance, respectively.

Furthermore, this may also be attributed to the fact that larger  $G_r$  values have more flux leakage and higher operating frequency which in turn give rise to synchronous reactance, hence the lower power factor. Doing the comparison between the three machine types, overlap winding PMVMs shows better power factor relative to the other two machine types. This is because the tooth concentrated winding machines have more magnetic reluctance due to the modulating pieces situated in-between the rotor and stator. Besides, most of the tooth concentrated-winding machines are characterized by poor winding factor. In general, the results in Fig. 4 demonstrate that the PMVMs' power factor at this output power capacity can hardly reach above 0.8, yet it can go as low as 0.4. Thus, the  $G_r$  does not only improve on the machines' torque capacity, but also scales up the reactance as proved by (7), leading to poor power factors. Therefore, continuous increase of pole-ratio would eventually lead to the significant decrease of power factor.

### C. Torque Quality

In PM excited and iron cored slotted machines, cogging and torque ripples are naturally caused by the PM field interaction with the slotted stator teeth permeance and stator electromagnetic field harmonics, respectively. Consequently, a good indication to the percentage magnitude of these performance index can be derived by examining the lowest common multiple (LCM) between the PM pole-pair and stator teeth numbers [15]. Theoretically, a higher LCM value is more favorable since it usually predicts lower degree of cogging or ripple torque. In this study, the torque ripple characteristics (shown in Fig. 5) were calculated using the multi-step static FEA.

It is interesting to see how the percentage ripple torques are so small for most of the overlap winding PMVMs without any measure being applied to minimize them. This inherent feature, coming about as a result of high LCM between stator pole-pairs and slot numbers is one strong advantage of this machine type. On the other hand, the combinations with  $G_r = 5$  have the worst torque ripples across all the three machine types. The tooth concentrated winding PMVMs show significant torque ripple with most of them above 5% mark, and this is to be expected since this type of winding is well known to be rich in magnetic field harmonics.

## V. COMPARISON OF PMSM AND PMVM

For the comparative purposes, a previously designed PMSM machine was used as the benchmark to be analyzed with the best designed PMVM [16]. In order to do a fair comparison study on these two machines, the rated operating speed and output power were kept equal as 150rpm and 15kW, respectively. According to the results provided in section IV, the most favorable PMVM configuration among the three examined types was found to be the overlap-winding PMVM as it generally possess better power factor and lower torque ripples. The main properties of the two machines are described in Table IV and their cross sections provided in Fig. 6. In addition, the two generators' detailed dimensional parameters are also given in Table V.

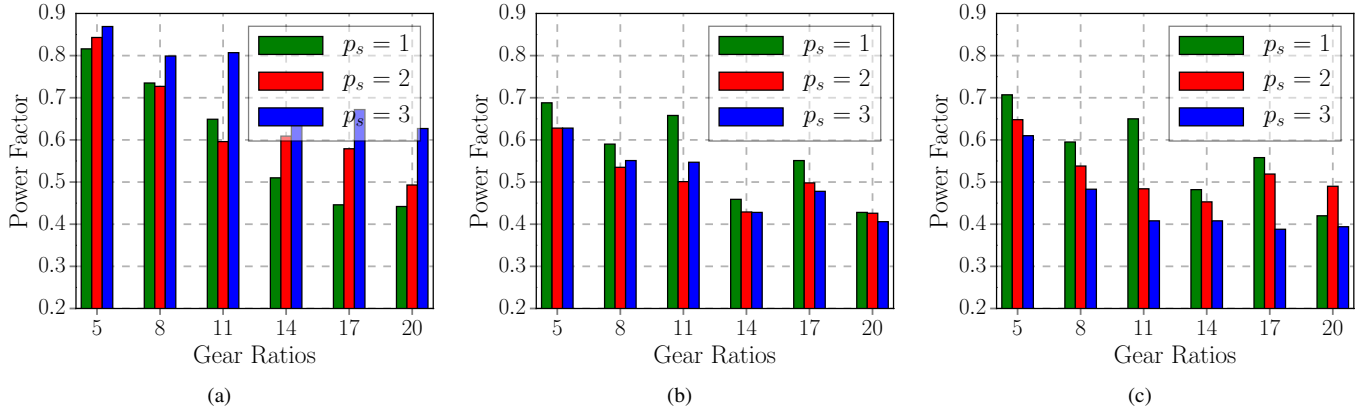


Fig. 4. Power factor vs Gear ratio.: (a) Conventional overlap-winding PMVM (b) Tooth concentrated, split tooth PMVM (c) Tooth concentrated, separate modulator PMVM.

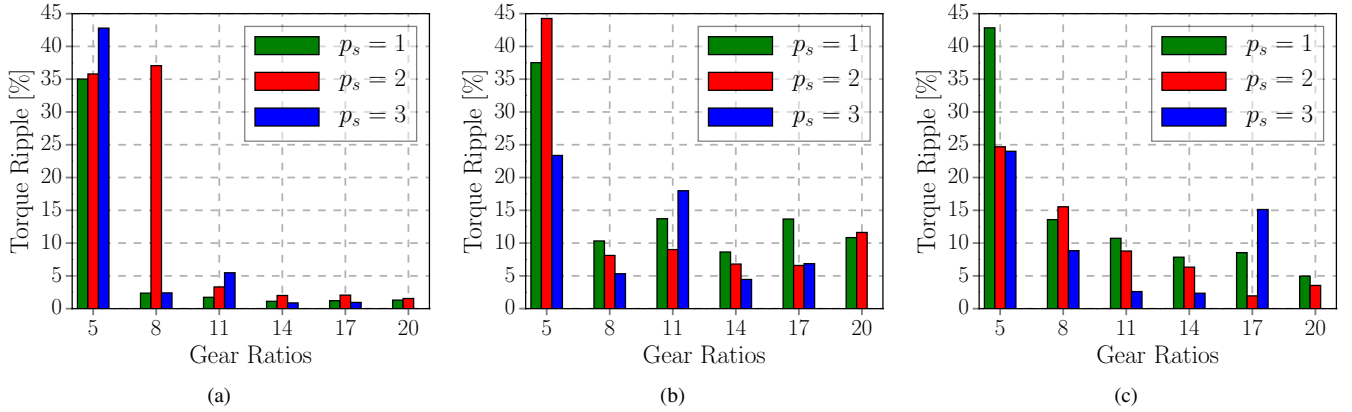


Fig. 5. Torque ripple vs Gear ratio.: (a) Conventional overlap-winding PMVM (b) Tooth concentrated, split tooth PMVM (c) Tooth concentrated, separate modulator PMVM.

TABLE IV  
COMPARED MACHINE PROPERTIES.

Parameter	PMSM	PMVM
Stator slots	48	36
Winding poles	40	6
Rotor poles	40	66
Rated frequency (Hz)	50	82.5
Winding type	Tooth concentrated	Overlapping

TABLE V  
MACHINES' DIMENSIONAL PARAMETERS.

Parameter	PMSM	PMVM
Rotor yoke height ( $t_{ry}$ )	8.3 mm	13.6 mm
Rotor magnet height ( $t_{mh}$ )	5.5 mm	3.9 mm
Magnet pole span ( $\sigma_{pm}$ )	0.84	0.88
Air-gap length ( $g$ )	2 mm	1.5 mm
Stator yoke height ( $t_{sy}$ )	6.7 mm	13.6 mm
Stator slot angle ratio ( $\sigma_s$ )	0.51	0.74
Slot opening ratio ( $\sigma_{so}$ )	1.0	0.82
Stator tooth length ( $l_{st}$ )	41.0 mm	27.96 mm

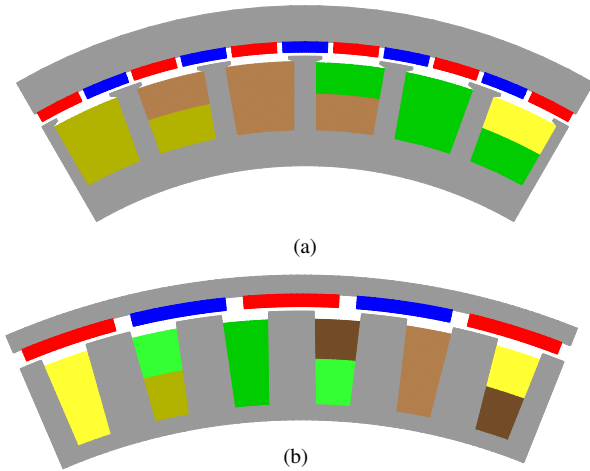
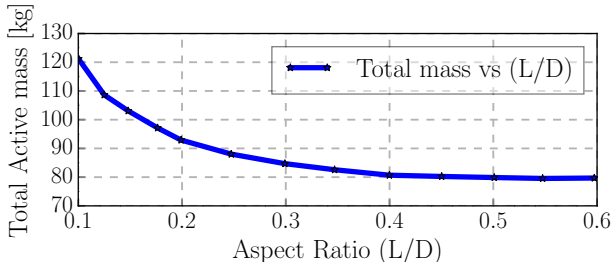
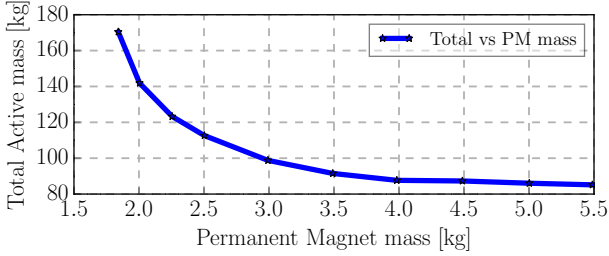


Fig. 6. Machine cross sections: (a) PMVM (b) PMSM.

For the PMVM, it was realized during the optimization process that the total active mass also varies greatly with the aspect ratio. Therefore, the influence of this variable on total active mass at a 15 kW level was investigated on a machine with  $p_s = 3$ ,  $p_r = 33$  and  $Q = 36$ . As can be read from Fig. 7a, the PMVM's mass is high at very low aspect ratios, but this tends to decrease with increasing ( $L/D$ ) values. From 0.4 to 0.6 the mass remains almost constant, which means 0.4 would be the best aspect ratio for this machine. Another relation to explore was the total active mass versus PM mass. While the overall weight of the machine is an important aspect for the intended application, the cost per kilogram of PM mass is usually high, hence it has a



(a)

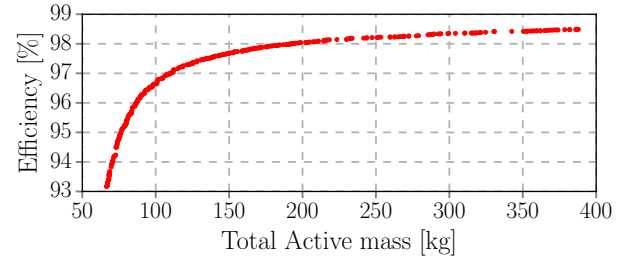


(b)

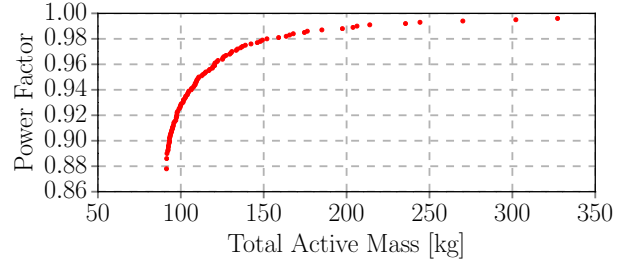
Fig. 7. Total mass vs.: (a) aspect ratio and (b) PM mass.

significant contribution to the cost of the machine. The plot of the relationship between these two masses is provided in Fig. 7b, and it shows that small PM material usage renders the heaviest machine. But with the increase of the PM mass, the total active mass rapidly decreases before it gets stagnant at 4.0kg of PM mass and beyond. According to this graph, the highest PM mass required for this machine type and output capacity, would be around 5.5kg, with the total active mass being just over 80kg. This is arguably an advantage for the PMVM when compared to the normal PM synchronous machines as the latter usually require more PM material.

A more sophisticated approach of doing the similar design as in Fig. 7 would be to perform a multi-objective optimization whereby an objective function is defined as a vector of two or more performance indexes. That is, all elements of the vector objective function are simultaneously optimized to find a set of variables satisfying all the inequality or equality constraints imposed on the search space. This gives a cluster of solutions from which one can select the best optimized points called Pareto optimal points. A Pareto front can then be obtained by plotting a set of Pareto optimal points in an objective space of two elements of vector objective function. It gives a boundary between the feasible and infeasible design options. Non-dominated Sorting Genetic Algorithm II (NSGA II) was implemented as a non-gradient based optimization strategy for the multi-objective design. Fig. 8a shows the Pareto-front found between efficiency and total active mass defined as the two objectives, where the trade-offs can be clearly seen. It shows that the total active mass increases in accordance with increasing efficiency. The reason behind this is that, to improve on the efficiency, both the magnetic and electrical loadings have to be lowered, and that can easily be achieved by having thicker yokes (more core mass) and more winding mass. But with increasing the



(a)



(b)

Fig. 8. Total mass vs.: (a) efficiency and (b) power factor.

mass to reduce the electromagnetic loading, the efficiency can only be increased up to a certain level after which it remains almost constant. This is due to the winding resistance and reactance, especially that of the end-winding, which leads to overwhelming losses which in turn affects the efficiency. Therefore, the graphs dictates that there can be no other design points that can have higher efficiency than the boundary indicated by the Pareto-front for this machine type with the previously defined specifications. It was also important to investigate the feasibility of improving on the power factor of PMVM since it normally ranges on the lower side of the scale. As it was done with efficiency, the Pareto-front line was drawn between the power factor and total active mass in Fig. 8b.

Regarding the comparison of the two machines, an estimation of the active volumetric machine size can be given by the total diameter ( $D_{out}$ ) and active stack length ( $L_{stk}$ ). While the active volume of the PMVM is about 60% of that of the PMSM, the total volume of the PMVM is close to 72% of the PMSM when taking into account their respective end-winding overhang. Even though the PMVM has about 50% more armature winding mass than the PMSM, due to its long end-winding, it still has slightly less overall total active mass than its counterpart. Moreover, it uses approximately 30% less PM material than that of PMSM. Output efficiencies are almost equal since this was the minimum requirement constraint for the design optimization. The PMSM has a high power factor, which is normal for synchronous PM machines, whereas the PMVM has a lower power factor of 0.78. This is a known disadvantage for PMVMs, and with the above indicated power factors, it can result in a converter system cost increase of about \$24 based on the prices of SEMIKRON IGBT power modules. As a result, the PMVM's lower cost merit will be somewhat discounted since

TABLE VI  
COMPARISON OF PMSM AND PMVM.

Parameter	PMSM	PMVM
Maximum torque ( $T_{avg}$ )	1000.0 Nm	1014.0 Nm
Torque ripple ( $T_{rip}$ )	3.42 %	1.25 %
Cogging torque ( $T_{cogg}$ )	2.34 %	1.66 %
Winding losses ( $P_{cu}$ )	588.48 W	480.4 W
Core Losses ( $P_{core}$ )	252.19 W	320.9 W
PM losses ( $P_{PM}$ )	109.31 W	155.47 W
Output power ( $P_{out}$ )	15.0 kW	15.4 kW
Efficiency ( $\eta$ )	94.44 %	94.2 %
Power factor (PF)	0.97	0.78
Outer diameter ( $D_{out}$ )	655 mm	433 mm
Stack length ( $L_{stk}$ )	125 mm	151 mm
End-winding overhang	23 mm	66 mm
Inner diameter ( $D_i$ )	528 mm	313 mm
PM mass (\$50/kg)	7.0 kg	4.85 kg
Silicon steel mass (\$2/kg)	62.44 kg	45.08 kg
Copper mass (\$6.67/kg)	20.16 kg	34.49 kg
Total mass	89.6 kg	84.42 kg
Total active material cost	608 \$	563 \$

the total sum of the generator and converter costs will end up being similar between these two systems. Cogging and torque ripple are two other critical factors in PM machines, as they can affect the machine's starting capability and also create adverse mechanical vibration and noise. The PMVM has smoother torque output than that of the PMSM as evidenced in Table VI.

## VI. CONCLUSION

A comparative study between two surface mounted PM machines, a PMSM and a PMVM, has been conducted in this paper. Since the PMSM was already existing and taken as the comparison benchmark, the study began by designing the PMVM with more emphasis placed on the effect of pole-ratio on certain performance indexes. Therefore, it was shown that careful consideration needs to be applied when choosing the pole/slot combination of PMVM because that is one of the major determining factors for the machine's total active mass, power factor and torque quality. From the comparison results, the designed PMVM has a clear advantage of lower PM material requirement while also boasting on the smaller cogging and ripple torques. On the other hand, the PMSM has good power factor which makes it to be logically better on the size, cost and operational losses of the converter relative to the PMVM. Based on the presented results, the PMVM can be deemed a reasonable alternative to its PMSM counterpart at the investigated output power level.

## REFERENCES

[1] G. Shrestha, H. Polinder, and J.A. Ferreira, "Scaling laws for direct drive generators in wind turbines," in *IEEE Int'l Electric Machines and Drives Conf.*, pp. 797–803, May 2009.

[2] H. Li and Z. Chen, "Overview of different wind generator systems and their comparisons," *Renewable Power Generation, IET*, vol. 2, no. 2, pp. 123–138, June 2008.

[3] H. Polinder, F. Van der Pijl, G.-J. de Vilder, and P. Tavner, "Comparison of direct-drive and geared generator concepts for wind turbines," in *IEEE Int'l Conf. on Electric Machines and Drives*, pp. 543–550, 2005.

[4] B. Kim and T. A. Lipo, "Operation and design principles of a PM vernier motor," *IEEE Trans. Ind. Appl.*, vol. 50, no. 6, pp. 3656–3663, Nov. 2014.

[5] J. Li and K. Chau, "Performance and cost comparison of permanent-magnet vernier machines," *IEEE Trans. Appl. Supercond.*, vol. 22, no. 3, ASN: 5202304, June 2012.

[6] W. Fu and S. Ho, "A quantitative comparative analysis of a novel flux-modulated permanent-magnet motor for low-speed drive," *IEEE Trans. Magn.*, vol. 46, no. 1, pp. 127–134, Jan. 2010.

[7] C. Liu, C. H. Lee, and M. Chen, "Comparison of outer-rotor permanent magnet machines for in-wheel drives," in *IEEE Int'l Symp. on Industrial Electronics (ISIE)*, pp. 1–6, May 2013.

[8] S. Gerber and R.-J. Wang, "Design and evaluation of a PM vernier machine," in *IEEE Energy Conversion Congress and Exposition (ECCE)*, pp. 5188–5194, Sept. 2015.

[9] B. Kim and T. A. Lipo, "Design of a surface PM vernier motor for a practical variable speed application," in *IEEE Energy Conversion Congress and Exposition (ECCE)*, pp. 776–783, Sept. 2015.

[10] A. Toba and T. A. Lipo, "Generic torque-maximizing design methodology of surface permanent-magnet vernier machine," *IEEE Trans. Ind. Appl.*, vol. 36, no. 6, pp. 1539–1546, Nov. 2000.

[11] S. E. Skaar, Ø. Krøvel, and R. Nilssen, "Distribution, coil-span and winding factors for PM machines with concentrated windings," in *Int'l Conf. on Electrical Machines (ICEM)*, Sept. 2006.

[12] F. Libert and J. Soulard, "Investigation on pole-slot combinations for permanent-magnet machines with concentrated windings," in *Int'l Conf. on Electrical Machines (ICEM)*, Sept. 2004.

[13] Vanderplaats Research & Development, Inc, "Theory manual," 2013, June. [Online]. Available: <http://www.vrand.com/visualDOC.html>

[14] D. Li, R. Qu, and T. A. Lipo, "High-power-factor vernier permanent-magnet machines," *IEEE Trans. Ind. Appl.*, vol. 50, no. 6, pp. 3664–3674, Nov. 2014.

[15] Z. Q. Zhu and D. Howe, "Influence of design parameters on cogging torque in permanent magnet machines," *IEEE Trans. Energy Convers.*, vol. 15, no. 4, pp. 407–412, Dec. 2000.

[16] J. H. J. Potgieter and M. J. Kamper, "Design optimization of directly grid-connected PM machines for wind energy applications," *IEEE Trans. Ind. Appl.*, vol. 51, no. 4, pp. 2949–2958, July 2015.

## VII. BIOGRAPHIES

**Pushman M. Tlali** was born in Leribe, Lesotho in 1987. He received his BEng in Electrical and Electronic Engineering at Stellenbosch University, South Africa in 2012 and his MEng in 2015. He is currently pursuing his PhD in the field of electrical machines, with specific focus on permanent magnet vernier machines. His research interests are in the design of magnetically geared electrical machines and renewable energy power generation.

**Rong-Jie Wang** received his PhD degree in Electrical Engineering from Stellenbosch University in 2003 where he is currently an Associate Professor. His research interests include special electrical machines, computer-aided design and optimization of electrical machines, thermal modeling of electrical machines and renewable energy systems. He was a co-author of the monograph *Axial Flux Permanent Magnet Brushless Machines* (Springer).

**Stiaan Gerber** was born in Bellville in South Africa on February 20, 1986. He received his PhD in Electrical Engineering at Stellenbosch University in 2015 where he is currently working as a post-doctoral researcher. His main interests in the engineering field are electrical machine design, numerical optimization, renewable energy power generation and finite element methods.